EPJ Web of Conferences **376**, 01005 (2026) https://doi.org/10.1051/epjconf/202637601005
*ICRAMEN 2026*

# Sustainable Green Synthesis of Supported $Fe_3O_4/SiO_2/AgVO_3$ Magnetic Nanocomposites for High-Efficiency Removal of Textile Dyes and Recyclable Environmental Remediation

*Alaa* Waleed Juma[1], *Nuralhuda* Aladdin Jasim[2*], *Alaa* Kharbat Shadhar[2]

[1] Environmental and water engineering department, College of Engineering, Wasit University,
[2] Civil Engineering Department, College of Engineering, Wasit University,

**Abstract.** The synthetic color emissions from the rapidly expanding textile sector are becoming increasingly concerning. Because they are toxic, long-lasting, and difficult for the environment to break down, these dyes are a big hazard. In order to create environmentally friendly and magnetically recoverable nanoparticles for water-based dye removal, this research used a green synthesis method to create magnetic nanocomposites based on $Fe_3O_4$ that were coated with $SiO_2$ and $AgVO_t$. The nanocomposites were created in two distinct structural arrangements: supported and core-shell. Due to its emphasis on chemical reduction, the green synthesis pathway provided an improvement over conventional preparation methods in terms of safety. Because it improved structural stability and active site dispersion, inserting the $SiO_2$ interlayer enhanced functional performance.Methylene blue was utilized to evaluate the photocatalytic effectiveness of the synthesized nanocomposites as a model synthetic dye pollutant. Good removal capability was demonstrated by both the core-shell and supported designs, although the supported $Fe_tO_4/SiO_2/AgVO_t$ nanocomposite outperformed the others due to the easier accessibility of reactive sites. To find the optimal conditions, we evaluated the effects of critical operating factors like light intensity, starting dye concentration, pH of the solution, nanocomposite dosage, hydrogen peroxide concentration, and reaction temperature in depth. Results from reusability tests, which demonstrated no degradation in performance over five cycles, provided further evidence of the nanocomposite's recyclability and durability. The degradation process was further clarified by conducting scavenger tests, which helped identify the reactive species that were most frequent. These nanoparticles offer a lot of potential as effective and environmentally safe instruments for restoring degraded ecosystems and enhancing wastewater treatment.

* Corresponding Author Email: njasim@uowasit.edu.iq

# 1 Introduction

Modern environmental restoration relies heavily on water purification. The increasing presence of both organic and inorganic contaminants in wastewater streams is mostly attributable to human activities. The use of disinfectants, pesticides, industrial dyes, pharmaceutical compounds, and agricultural fertilizers are all instances of such pollutants [21,22]. Goodarzi, Ashrafi-Peyman, Khani, and Moshfegh (2023) state that Figure 1 graphically represents the origins of inorganic and organic water contamination. A dye is an aromatic molecule that contains a colorant that absorbs light and produces a visible-light hue [1,2]. Over 100,000 kg of commercial dyes are recorded annually, ranging from 7 × 10^8 to 1 × 10^9 kg [3]. The first synthetic dye, which went by the name "Mauveine," was made in 1856 by William Henry Perkin. A natural aniline dye, it was called [4]. Permanent dyes can be used to color substances such that they do not fade when exposed to elements including water, light, oxidizing agents, sweat, and bacteria [5]. Food, rubber, printing, cosmetics, medicine, plastic, concrete, paper, and many more industries find diverse uses for colors due to these benefits [6-8]. The wastewater produced by these companies is unbefitting for human consumption due to the contamination it contains with carcinogenic compounds and toxic dyes. The textile industry uses more dye than any other sector, and the variety and complexity of the dyes it employs are unparalleled [10]. Paper, wool, silk, and cotton are all commonly dyed with methylene blue (MB), however this process requires a lot of energy [11–13]. According to Scopus, MB has several distinct applications. The number of studies addressing the degradation of MB dye increased consistently from 2010 to 2020, as seen in Figure 2. The molecular weight of MB is 319.85 g/mol, and it is an aromatic heterocyclic structure basic dye [20,21].A well-known cationic primary thiazine dye, MB, with the molecular formula C16H18N3ClS and a maximum absorption wavelength of 663 nm. At room temperature, it forms a stable solution with water due to its high solubility in the liquid [22-25].

One of the polymethine dye families, MB is a positively charged molecule that contains an aminoautochrome unit [26]. The chemical name is [3,7] -bis (dimethylamino) phenothiazine chloride tetramethylthionine chloride], as stated by the International Union of Pure and Applied Chemistry (IUPAC)[27,28].The molecular structure of the model and MB is shown in Figure 3. Many modern environmental restoration efforts emphasize the importance of water filtration (Khan et al., 2022). A wide range of inorganic and organic compounds are finding their way into wastewater streams as a direct consequence of human activities. A number of pollutants have been identified, including disinfectants, pesticides, industrial colors, agricultural fertilizers, and medicinal chemicals [21,22]. Figure 1 (Goodarzi, Ashrafi-Peyman, Khani, & Moshfegh, 2023) provides a visual representation of the different types of organic and inorganic water contamination. Dyeing involves the absorption of light by colored aromatic organic molecules, which change the hue of the visible spectrum [1,2]. Every year, around 100,000 commercial dyes, weighing around 7 × 10^8-1 × 10^9 kg, are utilized [3]. It wasn't until 1856 that William Henry Perkin found the first synthetic dye, an organic aniline hue named Mauveine [4]. Permanent dyes can be used to color substances in a way that they do not fade whether exposed to light, water, oxidizing chemicals, sweat, or bacteria [5]. These advantages explain why a wide variety of colors are used in many different industries, including textiles, food, rubber, cosmetics, medicine, plastic, concrete, paper, but also many more [6-8].

These companies release toxic and perhaps cancerous dyes into the environment in their massive amounts of wastewater. The water is now unfit for human consumption due to this. Dye usage is highest in the textile industry, which requires a wide range of dyes that are themselves very complicated [10]. One of the most energy-intensive compounds used in the dye business is methylene blue, or MB. It is used to dye a wide variety of fabrics, such as

cotton, silk, wool, and paper [11–13]. Scopus records a plethora of MB applications. Figure 2 demonstrates that between 2010 and 2020, there was a steady increase in the number of papers covering the topic of MB dye degradation. As a basic dye, MB has a molecular weight of 319.85 g/mol [20,21]. Heterocyclic aromatic molecules are what this chemical is.A well-known cationic primary thiazine dye, MB has a maximum wavelength of 663 nm and the chemical formula C16H18N3ClS. Because of how well it dissolves in water, it forms a stable solution with water at room temperature [22-25].A polymethine dye with an aminoautochrome unit, MB is positively charged [26]. The chemical name given to it by the International Union of Pure and Applied Chemistry (IUPAC)[27,28] is [3,7-bis(dimethylamino)phenothiazinechloridetetramethylthioninechloride], and its color index (CI) is 52015.The MB molecule's model and structure are shown in Figure 1.

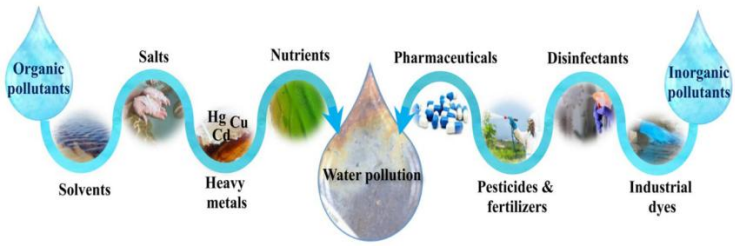


**Fig. 1.** Various organic and inorganic sources of water pollution in the environment

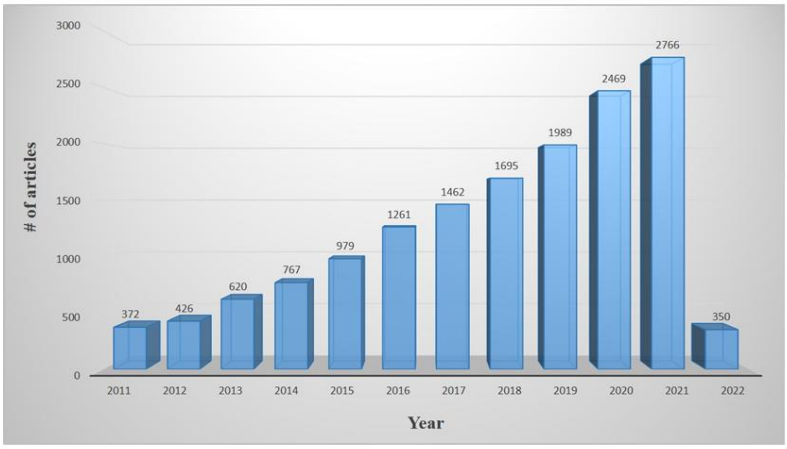


**Fig. 2 .** Annual article frequency as indicated by the Scopus database as of 12 January 2022 (Searched with the keyword 'methylene blue dye degradation').

The molecular weight of MB is 319.85 g/mol, and it is an aromatic heterocyclic structure basic dye [20,21]. MB is a well-known cationic primary thiazine dye due to its λmax at 665 nm and chemical composition C16H18N3ClS. At room temperature, it forms a stable solution with water due to its high solubility in the liquid [22-25]. One of the polymethine dye families, MB is a positively charged molecule that contains an aminoautochrome unit [26]. The chemical name is [3,7-bis(dimethylamino) phenothiazine chloride tetramethyl thionine chloride], as stated by the International Union of Pure and Applied Chemistry (IUPAC)[27,28]. The model and structure of the MB molecule are shown clearly in Figure 3 [29].

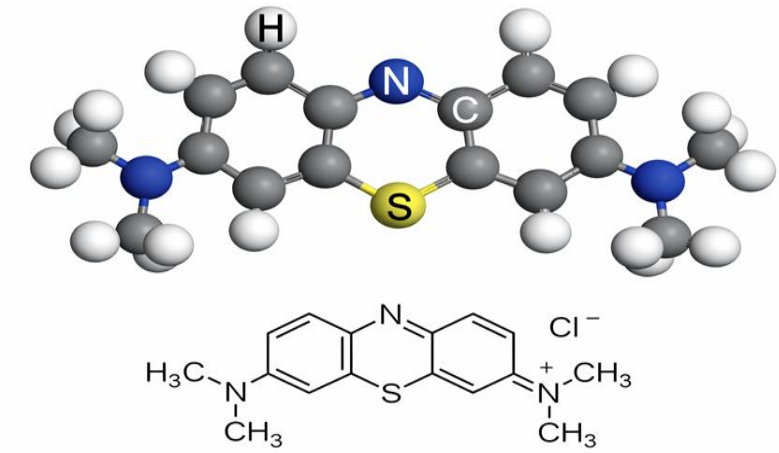


**Fig. 3** The model and the structure of the MB dye molecule [29] (Adapted with permission from the Royal Society). Society of Chemistry (license ID 1079849-1).

Recent decades have seen a rise in the use of multi-component photocatalysis of organic pollutants utilizing semiconducting NPs [166-168]. This technology is easy, cheap, and environmentally safe, making it an attractive option for cleaning wastewater that contains dangerous toxins. Thanks to its utilization of renewable energy and its cheaper catalysts, this technique outshines alternatives [169]. Industrial effluent dye removal relies on photocatalytic oxidation of MB to water and carbon dioxide [170]. Light is used in photodegradation, an oxidation process, to chemically degrade complex compounds into smaller, nontoxic, lower-molecular-weight fragments [171]. This innovative approach to wastewater treatment has the ability to decolorize wastewater by dissolving dye molecules into inert inorganic elements such as carbon dioxide and water [172]. This method can enhance a reaction rate without requiring the photocatalyst—a semiconductor material that is activated by light absorption—to be consumed (Khan et al., 2022). Because it is also a photocatalyst sensitizer, photodegradation of MB is an effective technique [180]. The photosensitized degradation of MB molecules when exposed to different light sources could be one reason why there is little breakdown of MB in the absence of catalysts [181,182]. Absorbing light in the 500-700 nm area, MB can undergo partial self-decomposition, generate singlet and triplet species, and experience electronic transitions and intersystem crossover [183]. Degradation of the MB dye requires O2 since it can be photolyzed in room temperature air. The production of •OH radicals occurs when MB+ radicals are monoelectron reduced by OH− in basic fluids. One of the most important active species in degradation reactions, H2O2, is formed when •OH react with one another. Similarly, when O2 interacts with excited MB* radicals, it forms O2•−. The photolysis mechanisms of MB are described by the following equations (1) to (3):

$$MB+ + OH- \rightarrow MB^* + OH\bullet \quad (1)$$

$$2OH\bullet \rightarrow H2O2 \quad (2)$$

$$MB^* + O2 \rightarrow MB+ + O2\bullet- \quad (3)$$

All these reactive radical species participate in the direct photolysis of the MB dye [179].

# 2. Substances and techniques

## 2.1. Components

No further purification was performed on any of the compounds; they were all utilized in their exact quantitative forms. This inquiry made use of the following resources: The following ingredients are used: histidine, also known as ferric chloride, •6(H2O)(97%), ferrous sulfate heptahydrate (FeSO4), which is obtained from Thomas Baker in India: •7H2O (99%, Alpha Chemika, India), tetraethyl orthosilicate Si(OC2H5)4 (98%, Sigma-Aldrich, China), sodium hydroxide (NaOH, 99.88%, SDFCL), ethanol (C2H5OH, 100%, Thomas Baker), ammonia solution (NH4OH, 25%, Thomas Baker, India), hydrogen peroxide (H2O2, 35%, Panreac, China), hydrochloric acid (HCl, 35-38%, Thomas Baker), and methylene blue C16H18ClN3S (good, HiMedia). You can see the characteristics of the materials used in the experiments in Table 1.

**Table 1.** The characteristics of the laboratory reagents used in the experimental method.

| Chemicals | Chemical name | Purities | Manufacturer | Mol. Wt. |
|---|---|---|---|---|
| Ferric chloride hexahydrate | FeCl3·6H2O | 97% | Thomas Baker, India | 270.3 |
| Ferrous sulfate heptahydrate | FeSO4·7H2O | 99% | Alpha Chemika, India | 278.0 |
| Tetraethyl orthosilicate (TEOS) | Si(OC2H5)4 | 98% | Sigma-Aldrich, China | 208.3 |
| Sodium hydroxide | NaOH | 99.88% | SDFCL | 40.0 |
| Ethanol | C2H5OH | 100% | Thomas Baker | 46.07 |
| Ammonia solution | NH4OH | 25% | Thomas Baker, India | 35.05 |
| Hydrogen peroxide | H2O2 | 35% | Panreac, China | 34.01 |
| Hydrochloric acid | HCl | 35-38% | Thomas Baker | 36.46 |
| Methylene blue | C16H18ClN3S | Pure | HiMedia | 319.85 |
| Silver nitrates | AgNo3 | 99.8% | ODAEJUNG, China | 169.87 |
| Ammonium metavanadate | $NH_4VO_3$ | 99% | CDH Fine Chemicals India, | 116.98 |

## 2.2. Preparation of Mandarin Peel Extract

After purchasing clean mandarin peels from a local seller, we cleaned and sterilised them in an ethanol solution with a concentration of 77%. The peels were air-dried for one day, and then dried for another 72 hours in a hot-air oven set at 60°C. The 10 grams of powdered mandarin peel, which had been processed in an electric grinder, was carefully measured using an analytical balance (Ohaus Adventurer) and transferred to an Erlenmeyer flask. The flask was then filled with 150 mL of distilled water in order to synthesize Fe3O4 NPs. For two hours, the mixture was heated to 40°C with a magnetic stirrer running at 500 rpm. The extract was filtered twice using Whatman No. 1 filter paper and then preserved at 4 °C in an airtight glass bottle, as seen in Fig.4.


**Fig. 4** Preparation of Mandarin Peel Extract filterd.

## 2.3. Properties of Fe3O4 nanoparticles

In materials research, Fe3O4 NPs have shown promise due to their extraordinary characteristics (Shah et al., 2025). The exceptional thermal, optical, structural, physical, magnetic, and electrical properties of Fe3O4 NPs make them very versatile (Table 2).

**Table 2** General properties of Fe3O4 (magnetite).

| Property | **Value** |
|---|---|
| Molecular Formula | $Fe_3O_4$ |
| Color | Jet black |
| Melting Point | 1583–1597 (°C) |
| Saturation Magnetization (Ms) at 300 K | 92–100 [emu·g$^{-1}$] |
| Density | 5.18 (g/cm$^3$) |
| Type of Magnetism | Ferrimagnetic |
| Curie Temperature (Tc) | 858 (K) |
| Band Gap Energy (Eg) | 2.6 [eV] |
| Crystallographic System | Cubic |
| Structure Type | Inverse spinel |
| Lattice Parameter (nm) | α = b = c = 0.8396 |
| Lattice Angles | α = β = γ = 90° |
| Standard Gibbs Free Energy of Formation (ΔG$^o$f) | −1012.6 [kJ/mol] |

## 2.4 Synthesis of Fe3O4 MNPs

Fe2O3 magnetic nanoparticles (MNPs) were created using the co-precipitation method. The following molar ratios were maintained: 10 mL of deionized water was used to dissolve 0.25 mol (0.695 g) of $FeSO_4$•$7H_2O$, and 20 mL of deionized water was used to dissolve 0.25 mol (1.35 g) of $FeCL_n$•$6H_2O$. Adding 50 mL of mandarin peel extract followed the mixing of the two solutions in a glass beaker. Mixing the iron precursors with the extract required constant stirring for 30 minutes to ensure a complete interaction. Add $NH_4OH$ (12 M, 30 mL) dropwise to the mixture and stir for another hour at 80°C until the pH reaches 9-10. The precipitate was collected following a 10-minute centrifugation run at 5,000 rpm. After that, it was cleaned with ethanol to remove any surface or organic impurities that remained after being washed five times with deionized water. To prevent moisture loss, the specimen was dried in a hot air oven at 80°C for three to six hours (see Figure 5). After that, it was stored in an airtight container.

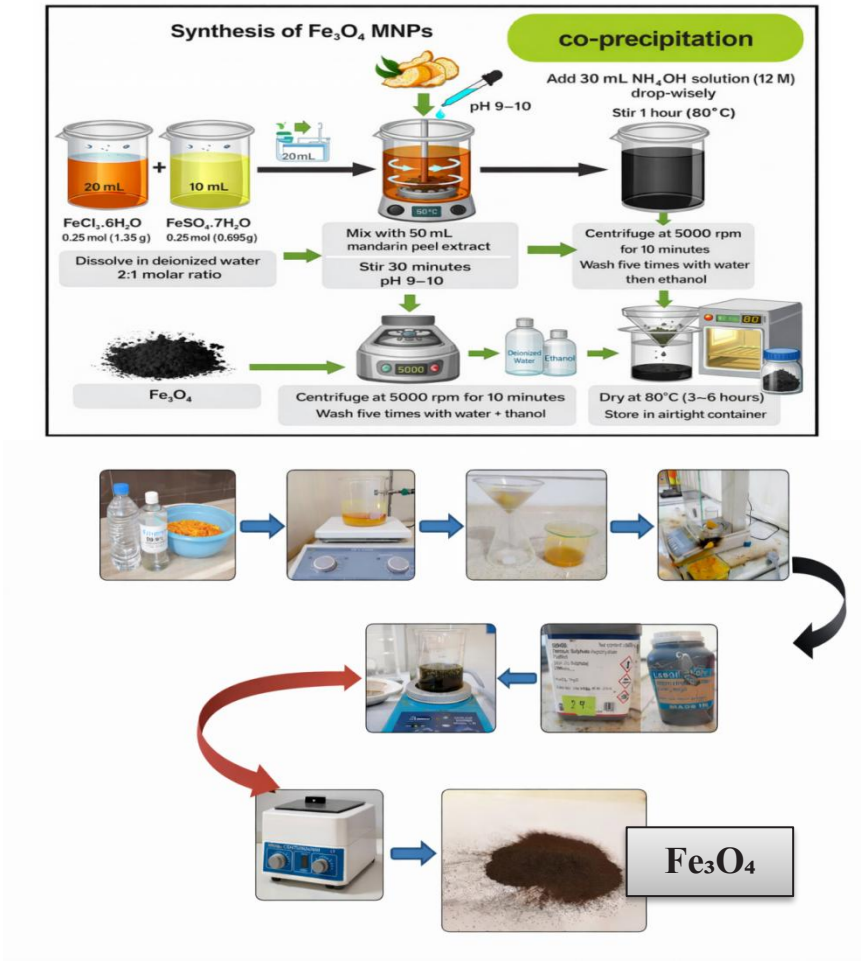


**Fig. 5** Synthesis of $Fe_3O_4$ Magnetic Nanoparticles (MNPs) via Co-precipitation.

## 2.5 Synthesis of Silver Vanadate $AgVO_3$

Nanoribbons made of silver vanadate ($AgVO_3$) were created using an easy hydrothermal process. Achieving an equimolar ratio of 0.050 M required constant mixing of the 25 mL water solutions of silver nitrate ($AgNO_3$) and ammonium metavanadate ($NH_4VO_3$) for 20 minutes. To facilitate the formation of nanoribbon structures, the resulting solution was homogenized using a magnetic stirrer, which also ensured that the reactants were spread equally. As seen in Figure 7.

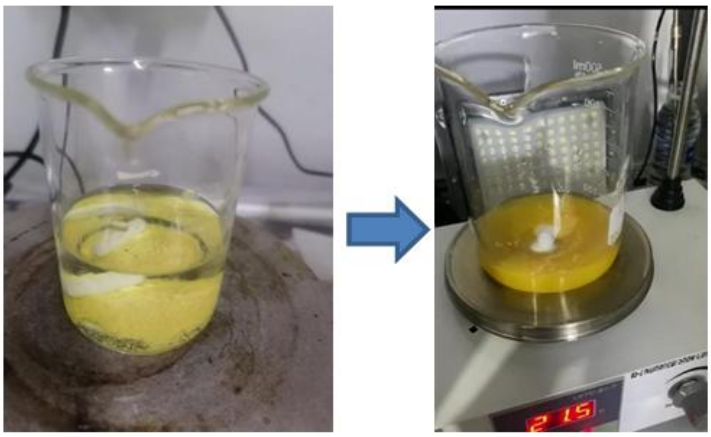

**Fig. 6** Synthesis of Silver Vanadate $AgVO_3$.

### 2.6 Assembly of $Fe_3O_4/SiO_2/AgVO_3$ Supported Nanocomposite Photocatalysts

In 50 mL of deionized water, the $Fe_tO_4$ nanoparticles covered with $SiO_2$ were suspended. After that, the suspension was supplemented with the AgVO3 nanoribbons that had been made earlier. To make sure the AgVO3 coating on the $Fe_tO_4/SiO_2$ surface was even, the mixture was stirred on a magnetic stirrer for three to four hours. A combination of deionized water and ethanol is used to wash the composite product multiple times after magnetic decantation is used for separation. The next step is to dry it for 12 hours at 60°C. Figure 8 demonstrates this.

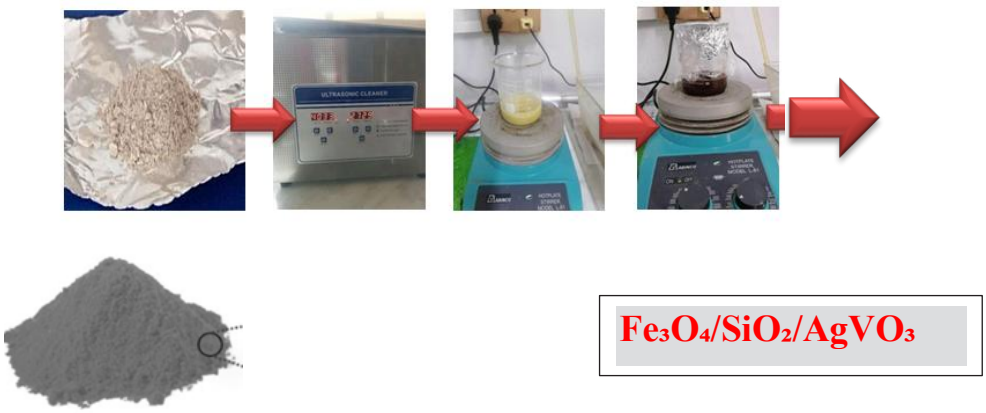


**Fig. 7.** Synthesis of $Fe_3O_4/SiO_2/AgVO_3$ Supported Nanocomposite Photocatalysts.

## 3. Characterization

### 3.1 TEM for ($Fe_3O_4/SiO_2/AgVO_3$ Supported Nanocomposite Photocatalysts

The produced nanocomposite $Fe_3O_4/SiO_2/AgVO_t$ has had its morphological and structural properties examined using transmission electron microscopy (TEM). Figures 8 show that the nanocomposite has a uniform structure with rod-like and somewhat amorphous particles. An even coating of $SiO_2$ covers the plainly visible $Fe_3O_4$ cores, which serve as the main scaffold.

For the subsequent deposition of $AgVO_3$ nanoparticles, the core-shell structure provides a solid foundation. The high-magnification scanning electron micrographs (Figure 8) of the $AgVO_3$ nanoparticles on $SiO_2$-coated $Fe_3O_4$ rods, which are small spherical clusters spaced along the rods' surfaces, demonstrate the effective surface functionalization. The particles in these $AgVO_t$ clusters are nanometer-sized, indicating that the composite components are integrated to a nanoscale level. Photocatalytic applications benefit from the nanocomposite's increased light absorption and charge separation made possible by its extremely porous and interconnected structure, as shown in the TEM photos.

The TEM images show that the $Fe_3O_4/SiO_2/AgVO_3$ nanocomposite was successfully synthesized; they also show that the nanoparticles are evenly dispersed and that the structure is intact, both of which are necessary for the photocatalytic application.

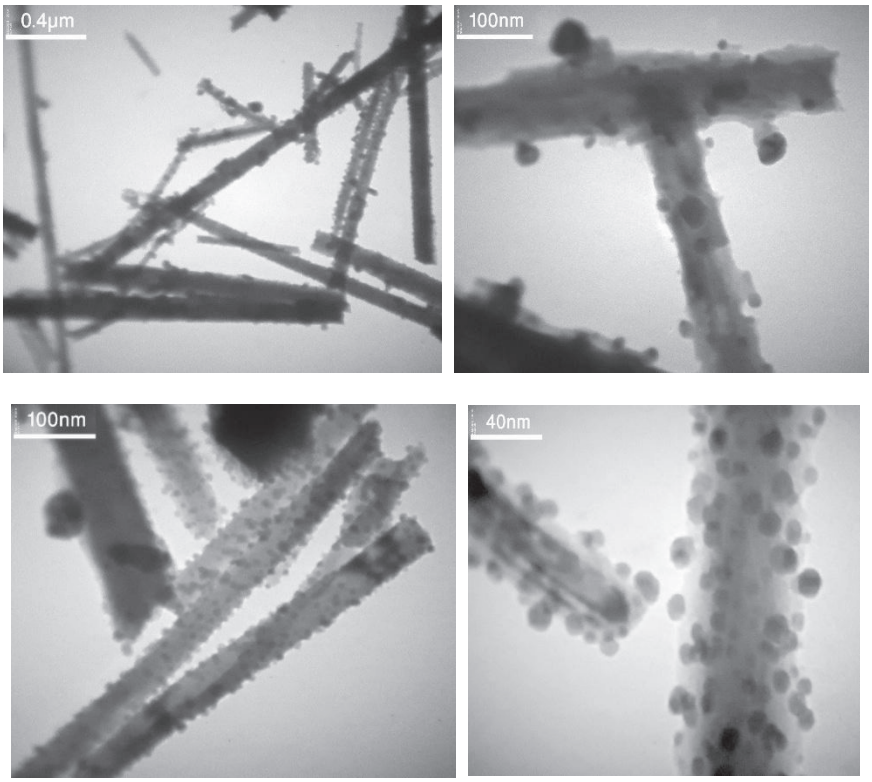


**Fig. 8**. The TEM image for ($Fe_3O_4/SiO_2/AgVO_3$ Supported Nanocomposite Photocatalysts.

### 3.2. FTIR for ($Fe_3O_4/SiO_2/AgVO_3$) Supported Nanocomposite Photocatalysts

Figure 9 displays the Fourier transform infrared spectra of $Fe_tO_4$, $Fe_tO_4$@$SiO_2$, and the supported $Fe_tO_4/SiO_2/AgVO_3$ nanocomposite. A recognized absorption band at 3431 $cm^{-3}$ is observed in the pure $Fe_3O_4$ spectra. This band is attributed to the O-H stretch of surface hydroxyl groups and/or adsorbed water molecules. The bending vibration band at 1628 $cm^{-1}$, which is designated as H-O-H, verified the presence of moisture. In addition, the peaks in the 400-600 $cm^{-3}$ range indicate the Fe-O stretching vibrations, providing further evidence of the well formed $Fe_3O_4$ core structure. The presence of hydrogen bonding interaction at the $Fe_tO_4/SiO_2$ interface is shown by a minor shift in the O-H stretching band to 3430 $cm^{-1}$ in the $Fe_tO_4$@$SiO_2$ spectra after coating with $SiO_2$. Si-O-Si stretching vibrations at 1101 $cm^{-1}$ and

bending vibrations at 1630 $cm^{-1}$ are novel bands in the spectra that demonstrate the creation of a silica shell surrounding the $Fe_3O_4$ core, respectively. Silica coating does not affect the observation of Fe-O vibrations, suggesting that the magnetic core structure remains intact. The produced $Fe_tO_4/SiO_2/AgVO_2$ nanocomposite shows additional absorption bands in its spectra compared to $Fe_tO_4@SiO_2$. The O-H stretching is nevertheless visible at 3431 $cm^{-1}$, and the Si-O-Si stretching is unaffected. The efficient incorporation of the vanadate species into the $Fe_3O_4/SiO_2$ framework is shown by the new bands at 647 $cm^{-1}$ and 478 $cm^{-1}$, which are ascribed as V-O stretching modes of $AgVO_3$. The composite's photocatalytic activity and structural stability may be enhanced as a result of interactions between $Fe_3O_4$, $SiO_2$, and $AgVO_3$, as indicated by the small shifts in the individual components' distinctive peaks. Taken together, FTIR results validate the nanocomposite's step-by-step production and the chemical attachment of $AgVO_3$ to the $Fe_tO_4@SiO_2$ base.

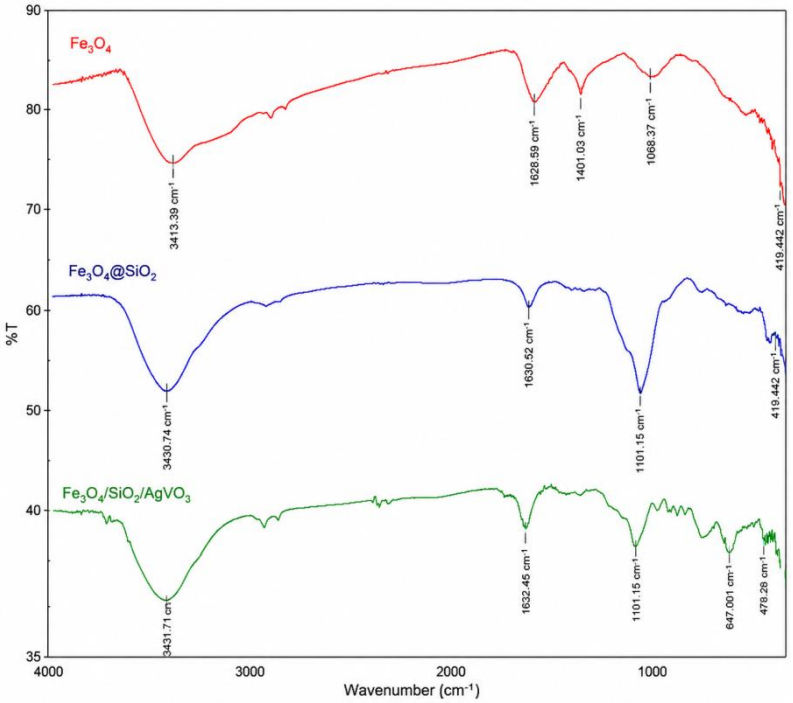


**Fig. 9** The FTIR Analysis of $Fe_3O_4$, $Fe_3O_4@SiO_2$, and $Fe_3O_4/SiO_2/AgVO_3$ Nanocomposite Photocatalysts.

### 3.3. VSM for ($Fe_3O_4/SiO_2/AgVO_3$) Supported Nanocomposite Photocatalysts.

Figure 10 shows the results of an investigation using vibrating sample magnetometry (VSM) into the magnetic characteristics of a $Fe_3O_4$, $Fe_3O_4@SiO_2$, and supported $Fe_3O_4/SiO_2/AgVO_3$ nanocomposite. The hysteresis loops exhibited superparamagnetic characteristics and are distinctively shaped as S-shaped loops in all three samples. The saturation magnetization of pure $Fe_3O_4$ is maximum due to the absence of any coating on the magnetic core, whereas that of $Fe_3O_4@SiO_2$ is lower due to the diamagnetic contribution of the silica shell. Because $AgVO_t$ is not magnetic and the composite gains mass, further addition of $AgVO_t$ to $Fe_tO_4@SiO_2$ reduces saturation magnetization very somewhat. Still, the samples' extremely low coercivity values point to their superparamagnetic nature, which is useful in contexts where a fast magnetic response free of residual magnetism is required. Thus, the magnetic interactions are affected by surface modification and functionalization,

with core characteristics being maintained. As a result, the magnetization of $Fe_3O_4$ gradually decreases to $Fe_3O_4$@$SiO_2$ and $Fe_3O_4/SiO_2/AgVO_3$. The VSM analysis demonstrated that the magnetic properties of the nanocomposite are maintained through the stepwise method of surface modifications, which is suitable for possible use in magnetic separation and catalytic applications. Additionally, the surface modifications change the size of the magnetization without affecting the basic superparamagnetic properties.

.

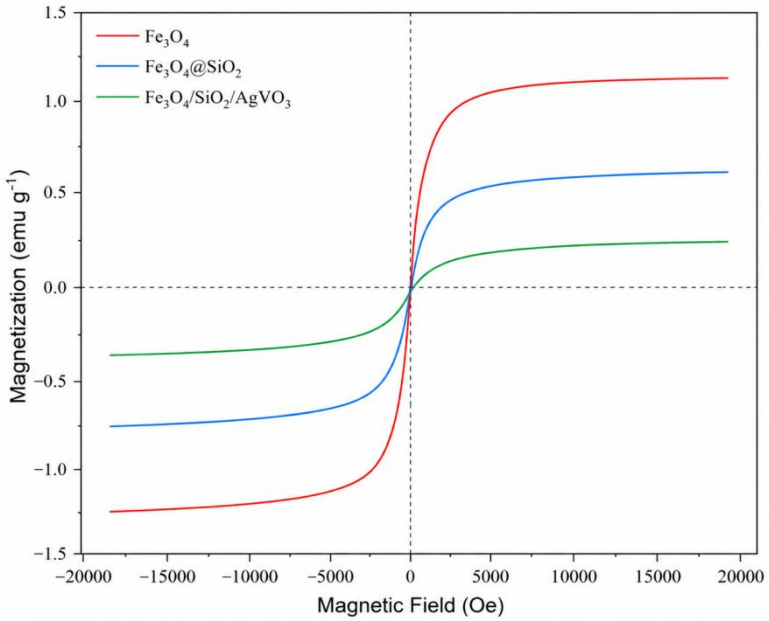


**Fig. 10** Magnetic Hysteresis Curves of $Fe_3O_4$, $Fe_3O_4$@$SiO_2$, and $Fe_3O_4/SiO_2/AgVO_3$ Nanocomposite Photocatalysts.

### 3.4. XRD for ($Fe_3O_4/SiO_2/AgVO_3$) Supported Nanocomposite Photocatalysts.

Figure 11 displays the XRD patterns of the nanocomposite supported by $Fe_3O_4$, $Fe_3O_4/SiO_2$, and $Fe_3O_4/SiO_2/AgVO_3$. The presence of distinct peaks at (220), (311), (400), (422), (511) and (440) in the diffraction pattern of $Fe_3O_4$ suggests that the nanoparticles of $Fe_3O_4$ have been effectively produced as crystalline particles, as is characteristic of a cubic spinel structure. In the $Fe_tO_4$@$SiO_2$ pattern, the crystal peaks from $Fe_tO_4$ are still visible, indicating that the $SiO_2$ coating has no effect on the core crystal structure. However, the lower angles display a broad peak, which is indicative of amorphous $SiO_2$. A couple of additional diffraction peaks emerged in the $Fe_tO_4/SiO_2/AgVO_t$ nanocomposite. These are ascribed to the crystalline planes of $AgVO_t$, suggesting that vanadate species have been deposited onto the $Fe_tO_4$@$SiO_2$ framework. The presence of the primary peaks of $Fe_3O_4$ in the ternary nanocomposite preparation suggests that the core structure has been preserved. The inclusion of non-magnetic layers of $SiO_2$ and $AgVO_3$ causes the $Fe_3O_4$ peaks to be somewhat weaker compared to the uncoated nanoparticles. It is crucial for the $Fe_3O_4$ core to maintain its crystalline integrity and for the successful integration of each component to be checked by XRD analysis. This is done for both magnetic and photocatalytic applications. The results of this investigation lead us to believe that the nanocomposite was created in a sequential method, and that it contains the crystalline and amorphous phases of $Fe_tO_4$, $SiO_2$, and $AgVO_t$.

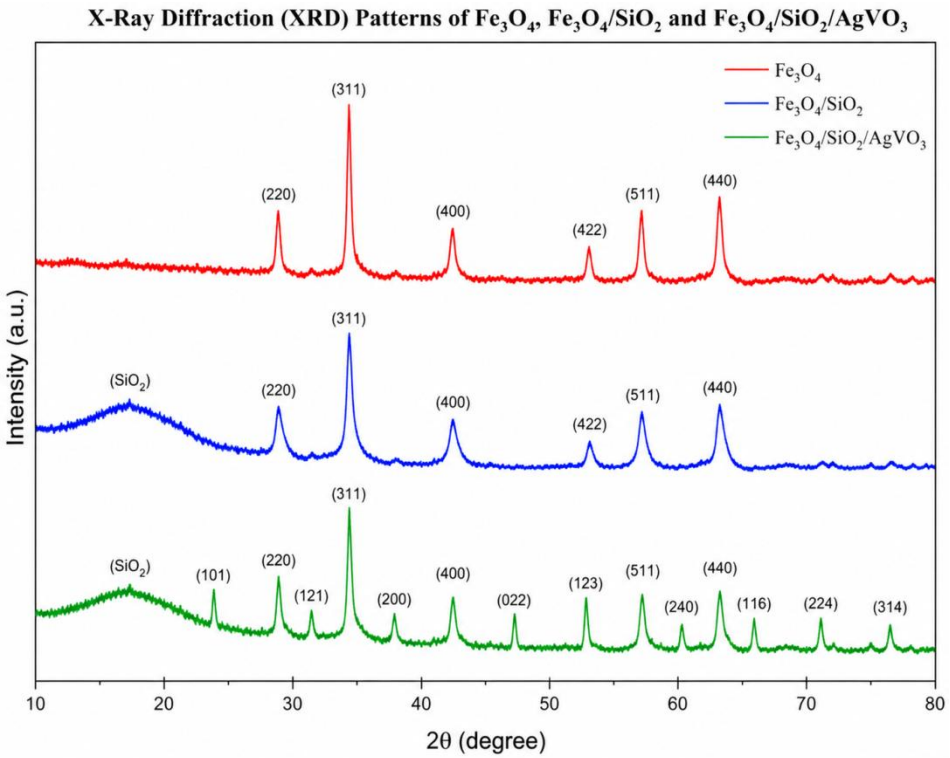


**Fig. 11** X-Ray Diffraction (XRD) Patterns of $Fe_3O_4$, $Fe_3O_4/SiO_2$, and $Fe_3O_4/SiO_2/AgVO_3$ Nanocomposites.

### 3.5. SEM for ($Fe_3O_4/SiO_2/AgVO_3$) Supported Nanocomposite Photocatalysts

The surface morphology and microstructural characteristics of $Fe_3O_3/SiO_2/AgVO_3$ nanocomposite were analyzed through the scanning electron microscopy (SEM). The nanocomposite has a well interconnected network of rods of uniform dimensions as shown in figures 12. Average rod length as measured from high magnification images (Figure 12) range from ~36.88 nm to 111.16 nm, which indicates that the nanorods were synthesized under controlled growth conditions. The SEM images show that there is no obvious agglomeration between the rods, and that the rod surfaces are highly dispersed, which is good for minimizing agglomeration and maximizing surface area. Such a morphology allows for efficient deposition of $AgVO_3$ nanoparticles, and guarantees that active sites are easily accessible for the photocatalytic reactions. The nanocomposite appears to be evenly distributed throughout the substrate at lower magnification (Figure 12) suggesting that a uniform composite structure has been formed with little clustering. In general, the SEM analysis shows that the $Fe_3O_4/SiO_2/AgVO_3$ nanocomposite is rod-like, has nanoscale dimensions, is uniformly dispersed, and is interconnected, properties that are desirable for increasing the photocatalytic efficiency by increasing the absorption of light, the transfer of charge, and the surface reactivity.

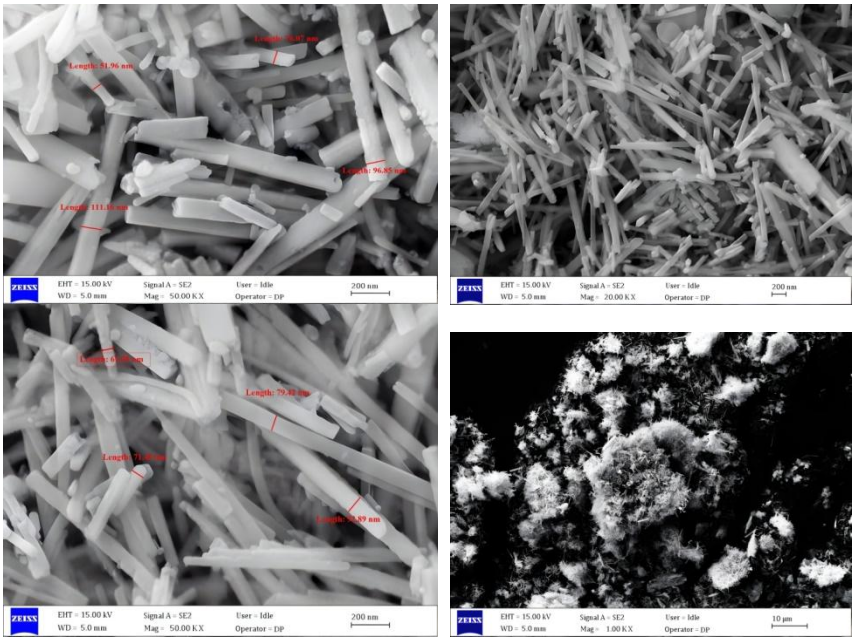

**Fig. 12** The SEM for ($Fe_3O_4/SiO_2/AgVO_3$) Supported Nanocomposite Photocatalysts.

## 4. Photocatalytic degradation experiments

Several materials, including ($Fe_tO_4$, $Fe_tO_4/SiO_2$, and **($Fe_3O_4/SiO_2/AgVO_3$)** supported), were tested for photocatalytic activity in a visible-light batch reactor. As seen in Figure 13. A batch experiment using Methylene Blue ($C_{16}H_{18}ClN_3S \cdot 3H_2O$) for photocatalytic degradation was part of the evaluation. In order to build a calibration curve for MB dye concentration, a UV spectrophotometer (UV-1200, China) was used to assess a range of standard aqueous MB dye solutions, from 1 to 50 ppm. A visible light source was used to illuminate the 100 mL glass beaker, which was used as the photocatalytic reactor.The visible lighting system consisted of three 50-watt LED bulbs in total. A mixer was used to evenly combine all of the reactor's components while also keeping the photocatalyst suspension in place. To initiate the photocatalytic degradation of MB, 100 mL of MB solution was added to an aqueous solution that already contained 40 ppm of MB. Afterwards, a range of nanocomposites were added to the solution at a concentration of 0.1 g/L. The resulting mixture was stirred for 180 minutes to reach absorption-desorption equilibrium. The reactor was then allowed to light for three hours after a total of 180 minutes of agitation. The UV-spectrometer (UV1200-Spectrophotometer) was used to capture a 3 mL sample at 665 nm intervals. Figure 4 shows a schematic representation of the photocatalytic breakdown of Rh B dye in the experimental investigation. The effects of the photocatalyst concentration, starting MB dye concentration, initial pH of the solution, and H2O2 concentration were also examined. The metal ferrites produced in previous studies were tested for their reusability and durability using five photocatalytic degradation cycles (Jasim, 2024 #8). After each iteration, the catalyst was taken out of the reaction solution and re-used following three washes with ethanol. Figure 13 displays the deterioration efficiency when subjected to VLI. The degradation performance (DP) of every photocatalyst was calculated using Equation 3.3.1 (Danish and Muneer, 2021).

$$DP\ (\%) = (C0 - Ct)/C0 \times 100 \quad (1)$$

In other words, where C0 is the initial concentration and Ct is the final concentration of the MB, as stated by Jasim et al. (2024). The effect of other parameters on the results was also examined. These included the concentration of the photocatalyst (0.5, 0.1, 0.15 g/L), the initial concentration of the MB dye (10, 40, 60 ppm), the initial pH of the solution (2, 4, 7, 10, and 12), and the concentration of H2O2 (120, 240, and 320 mM). A solution of 0.1 M NaOH and 0.1 M HCl was used to alter the pH. The synthesized photocatalysts were exposed to visible light for five cycles to investigate the MB stability and reusability. The photocatalyst that was utilized washed three times with ethanol and deionized water using a magnetic separator before being reused in the next cycle (Wu, 2021). Solution that has undergone photocatalysis.

For the purpose of studying the photocatalytic degradation of methylene blue (MB), many operational factors were meticulously examined. Considered parameters included the following: photocatalyst dosage (0.05, 0.10, and 0.15 g/L), starting MB concentration (10, 40, and 60 ppm), solution pH (2, 4, 7, 10, and 12), hydrogen peroxide concentration (120, 240, and 320 mM), light irradiation intensity (50, 100, and 150 W), and reaction temperature (25 C under ambient conditions and 60 °C). When necessary, we adjusted the pH of the solution using 0.1 M NaOH or 0.1 M HCl. Additionally, scavenger studies were carried out to identify the reactive species that primarily degraded MB. At a concentration of 0.5 mmol/L, certain scavengers like sodium oxalate ($Na_2C_2O_4$), potassium dichromate ($K_2Cr_2O_7$), sodium ethylenediaminetetraacetate ($Na_2EDTA$), p-benzoquinone ($C_6H_4O_2$), and isopropanol ($C_3H_8O$) were either included in the photocatalytic processes or not.

By exposing the synthesized photocatalyst to visible light for photocatalytic degradation for five consecutive cycles, its stability and reusability were evaluated. According to Wu (2021), after each cycle, the photocatalyst was extracted from the reaction mixture using a magnetic separator. It was then washed three times in a solution of ethanol and deionized water and reused in the following cycle.

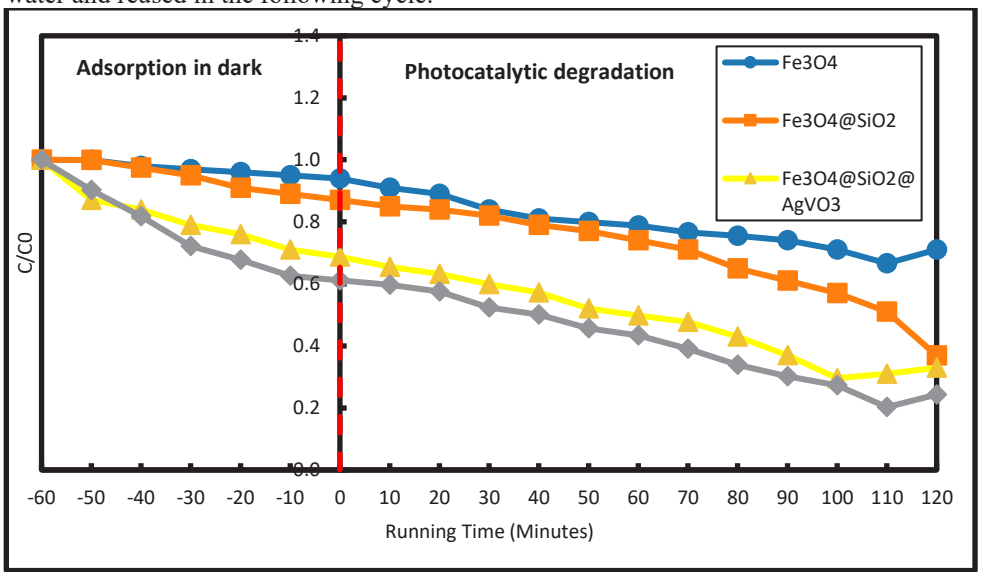


**Fig. 13** Removal Efficiency of Methylene Blue Over Time Using Catalysts without $H_2O_2$.and ph=5 : (a) $Fe_3O_4$ 33%, (b) $Fe_3O_4$@$SiO_2$ 62%, (c).$Fe_3O_4$@$SiO_2$@$AgVO_3$ cor&shell 70%, (d). $Fe_3O_4$/$SiO_2$/$AgVO_3$ supported 79%

**Fig. 14** A schematic representation of a photocatalytic batch reactor system designed for the degradation of (Rh B) dye using VLI

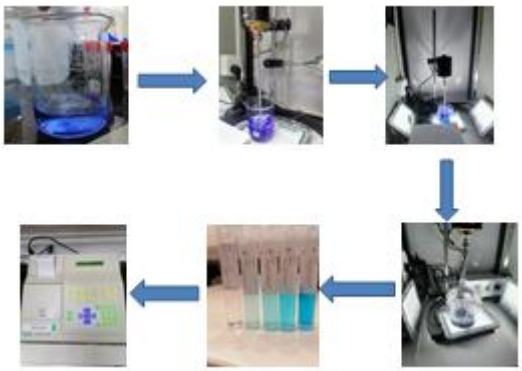

**Fig. 15**. The process of degradation efficiency under VLI

## 5.Photocatalytic performance assessment

### 5.1. The impact of the initial concentration of MB

Experiments were conducted with the following parameters: pH 10, 0.1 g of **($Fe_3O_4/SiO_2/AgVO_3$)** catalyst, and MB dye concentrations of 10, 40, and 60 ppm. The catalyst was exposed to 150W LED visible light for 10, 20, 30, 40, and 180 minutes, as shown in Figure 15. Below are the results. What matters most for the efficiency and speed of the photocatalytic process is the concentration of contaminants. This is thought by scientists to be caused by hydroxyl radicals (OH.) produced on the catalyst's surface, which react with the dye molecules and degrade them [40]. Because there are so many energetic sites on the surface of the photocatalyst, MB has an exceedingly high absorption capacity even at very low dye concentrations. An increase in the probability of MB interacting with OH* radicals at higher dye concentrations causes the initial breakdown rate of MB to rise with dye concentration [41]. Reaction kinetics are slowed down by an increase in MB collisions rather than OH* radical interactions as the MB level grows beyond 10 ppm [42]. Rising MB concentrations do cause degradation intermediates to form, according to Saraee, Maleki, Kikhavani, and Mansouri (2024). Inhibition of active OH* radical production by dye molecules occluding energetic areas on the surface of **($Fe_3O_4/SiO_2/AgVO_3$)** causes a decrease in photodegradation efficiency with increasing concentrations [43].

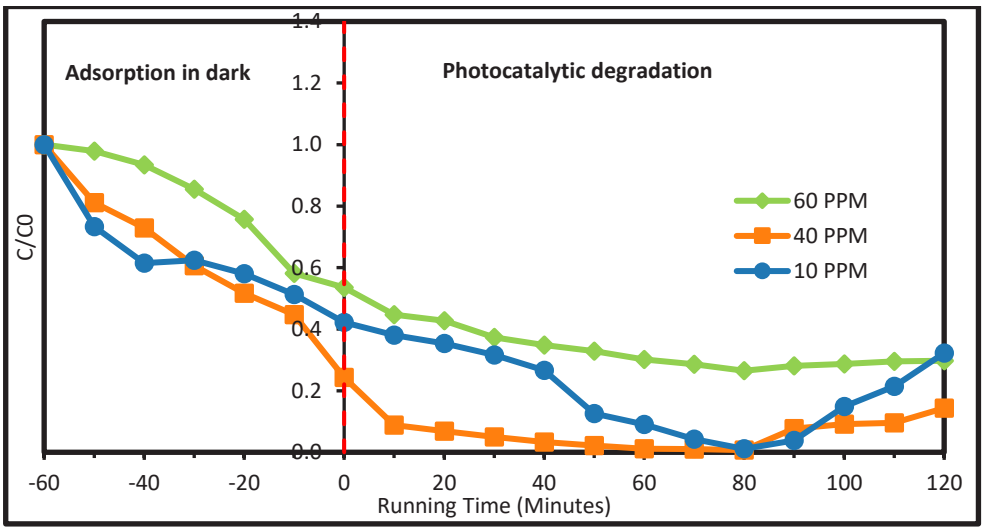


**Fig. 16** The effect of initial dye concentration on the removal of MB dye (pH=10, and 0.1 gm of catalyst, 120 mM of H2O2, exposed to 150 W LED visible light)

## 5.2. Impact of PH

The reaction fluid's pH has a significant impact on the photocatalytic process's efficiency [42]. While photocatalysts are capable catalysts, their effectiveness is limited to a narrow pH range since they are pH-dependent. Because changes in pH influence the charge characteristics of the catalyst surface and the molecular structure of the dye, these changes influence the degradation of the dye. Dye degradation rates are pH-dependent, with some colors dissolving more quickly in acidic settings and others being more easily removed by basic fluids [43,44]. Once the optimal methylene blue (MB) concentration was determined, the impact of pH could be examined by subjecting a catalyst dose of 0.1 g **($Fe_3O_4/SiO_2/AgVO_3$)** to 150 W of LED light for reaction durations within the 10–180 minute range at pH 2, 4, 7, 10, and 12. The results demonstrate that degradation efficiency is at its peak at a pH of 10, and it continues to rise as the pH rises. Figure 17 displays the results. When the pH drops below 6, the removal effectiveness is drastically diminished. This happens because of insufficient hydroxyl radical generation and unfavorable electrostatic interactions between the catalyst surface and the dye molecules. As a result, there is minimal adsorption and photocatalytic activity [43]. When operating in acidic environments, the system performs better when the solution contains a higher concentration of hydroxide ions (OH.). These ions facilitate the formation of the extremely reactive hydroxyl radicals and lend catalysts a negative charge. When the negatively charged surface of the catalyst comes into intense electrostatic contact with the positively charged MB molecules, photocatalytic degradation is accelerated. This improves adsorption because the majority of MB molecules are cationic in water [44]. (Esmail and colleagues' 2024 research). The efficacy of elimination becomes more noticeable as the pH rises above 10. The fundamental reason for this behavior is that there are too many OH ions. Dye molecules compete for active sites and there aren't enough highly oxidative •OH radicals available for the degradation stage. At a pH of 10, the current photocatalytic system is most effective at removing MB.

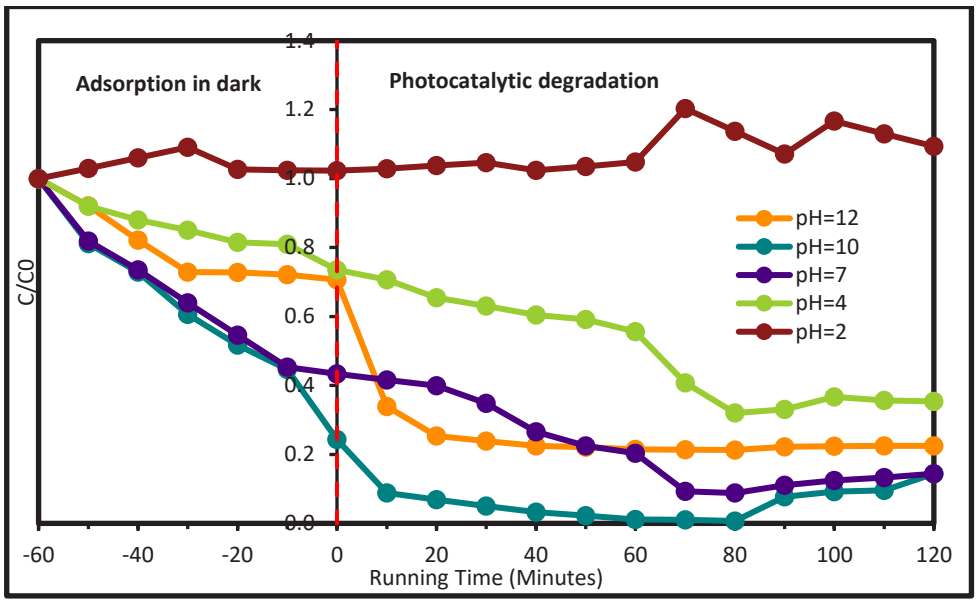


**Fig. 17** The impact of pH on the removal of MB dye (120 mM of H2O2, 0.1 g of catalyst dose, and 40ppm of MB dye initial concentration under 150W LED light).

### 5.3. Impact of H2O2

The effects of hydrogen peroxide ($H_kO_k$) on the elimination process were also studied. In their set of experiments, Jabbar et al. (2021) used a 40 ppm MB solution with a pH of 10, along with 0.1 g of the $Fe_tO_4/SiO_2/Ag_2VO_t$ catalyst. Under the illumination of 150 W LEDs, the solution was exposed to $H_2O_2$ concentrations ranging from 120 to 360 mM for reaction durations spanning from 10 to 180 minutes. Figure 18 displays the results. Adding $H_2O_2$ is an effective way to enhance the photocatalytic breakdown of MB. This is because hydroxyl radicals (•OH) are necessary for the oxidation of pigments, and hydrogen peroxide, a strong oxidizing agent, encourages their synthesis [44,45]. As is widely known, $H_2O_k$ can speed up degradation by producing 2 moles of •OH radicals through the correct photochemical reactions. The best degradation efficiency was observed at a concentration of 120 mM $H_2O_2$, suggesting that this may be the optimal dosage for the present system according to the experimental findings. Rapid molecular breakdown of MB occurs at this concentration due to the formation of •OH radicals. At doses higher than 120 mM $H_kO_2$, the efficiency of breakdown seems to diminish.

This decrease is mostly due by the scavenging action of copious $H_2O_2$ toward •OH radicals, as stated by Saraee et al. (2024). Hydroperoxyl radicals (•OOH) are very weak oxidizers that are produced when $H_2O_2$ reacts with •OH. In addition, an increase in radical-radical recombination and a decrease in photocatalysis efficiency might result from an excess of $H_2O_2$, which reduces degrading efficiency [45,47]. The optimal concentration for photocatalytic methylene blue removal, according to research, is 120 mM $H_2O_2$.

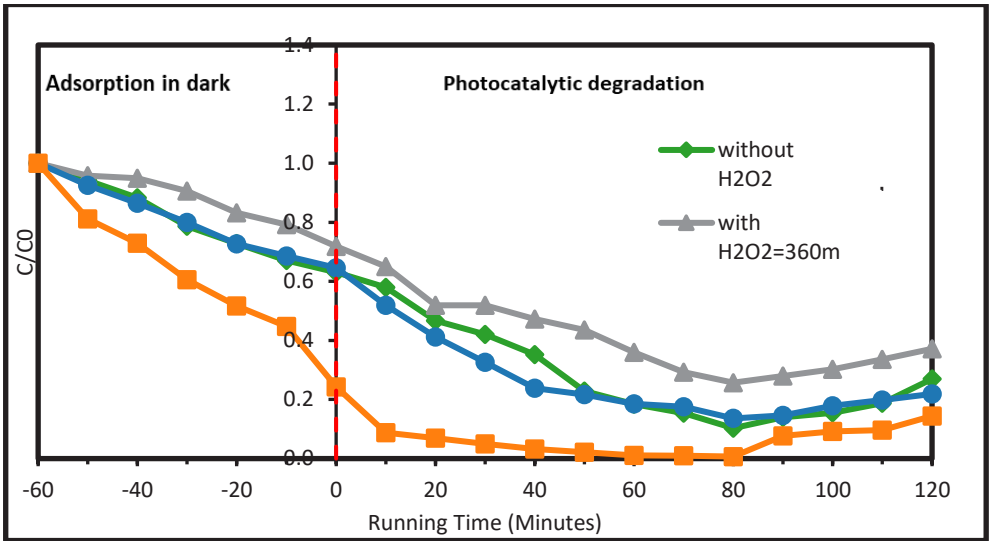


**Fig. 18** Effect of hydrogen peroxide ($H_2O_2$) on the photocatalytic degradation activity of MB dye for $Fe_3O_4/SiO_2/Ag_2VO_3$ at photocatalyst dose = 0.1 g/l, MB dye initial concentration = 40 ppm, initial pH = 10.

### 5.4. Effect of catalyst dose

While keeping the same working conditions of 40 ppm MB concentration, pH 10, and visible-light irradiation, the optimal dosage of the $Fe_tO_4/SiO_2/AgVO_3$ nanophotocatalyst was found by adjusting the dose to 0.05, 0.10, and 0.15 g. The results are displayed in Figure 19. To improve the efficiency of methylene blue removal, the dosage of the catalyst is increased to 0.10 g. The photocatalytic degradation rate is enhanced when the surface area and active site count are both increased, since this leads to better light absorption and faster reactive species generation [48,49]. On the flip side, removal efficiency decreases slightly when the catalyst dosage is increased to 0.15 g (Mohammed Elzatahry, Matalkeh, Al Soubaihi, and Saoud, 2023). Particles in suspension clump and solution turbidity increases with excessive catalyst loading, reducing light penetration and photocatalytic activity. The performance is declining because photogenerated charge carriers are not actively engaging in the process (Saraee et al., 2024). These findings stress the need of an adequate amount of light reaching the reaction medium and an adequate number of active sites. Under the current experimental conditions, it has been found that 0.10 g of $Fe_tO_4/SiO_2/Ag_2VO_t$ is the catalyst dose that maximizes MB removal efficiency [50,51].

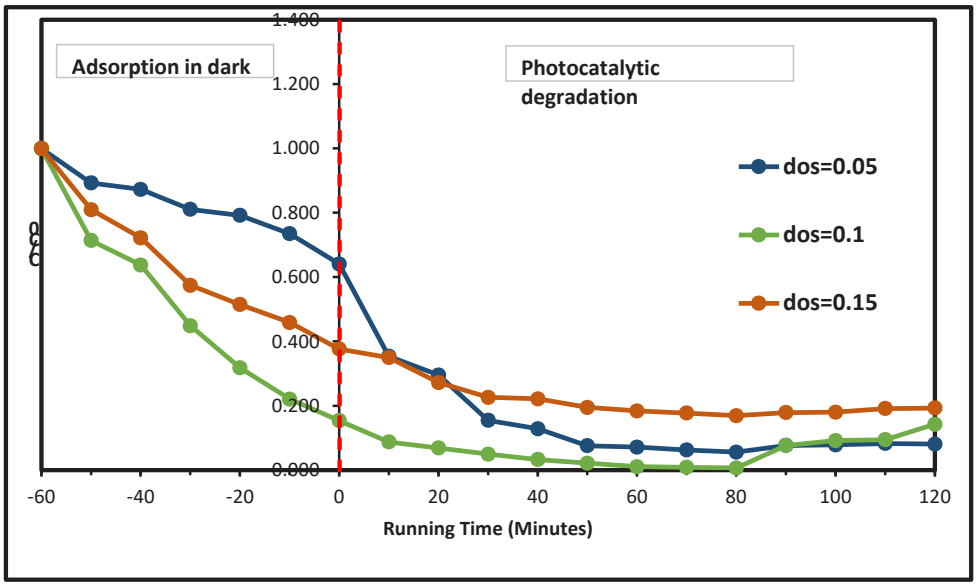


**Fig. 19** Effect of photocatalyst dose on the photocatalytic degradation activity of MB dye for $Fe_3O_4/SiO_2/Ag_2VO_3$ at photocatalyst dose = 0.05, 0.1, and 0.15 g/l, MB dye initial concentration = 40 ppm, initial pH = 10, and H2O2 concentration = 120 mM

## 5.5. Effect of Reaction Temperature

All other variables (light intensity, catalyst dosage, solution pH, and dye concentration) were kept constant, and the influence of reaction temperature was studied at both ambient temperature (25 °C) and 60 °C. At 25 °C, the data shows that methylene blue (MB) removal efficacy peaks, and at 60 °C, it starts to diminish dramatically. Maybe this phenomenon might be better understood if we consider that photocatalytic activities are primarily driven by light energy and not heat. The main reason why dyes degrade at higher temperatures is because fewer charge carriers are available to manufacture reactive species such hydroxyl radicals (•OH), as the recombination rate of photogenerated electron-hole pairs may be raised [2]. Figure 20 displays the outcomes. The efficiency of photocatalytic oxidation can be adversely affected by high temperatures because they reduce the stability of both hydrogen peroxide and the free radicals produced [12]. For the purpose of creating the optimal situation for optimizing MB removal, the combined outcomes of the assessed operational components were utilized. Temperature (25 °C), initial pollutant concentration (40 ppm), pH (10), and catalyst dose (0.1 g $Fe_tO_4/SiO_2/Ag_2VO_3$) were the best operating parameters for the photocatalytic system. Saraee et al. (2024) found that operating at moderate temperatures increased the photocatalytic system's stability and effectiveness. Working at excessively high temperatures has a negative impact on deterioration. Room temperature (25 °C) is therefore optimal for MB removal in this configuration [3, 4].

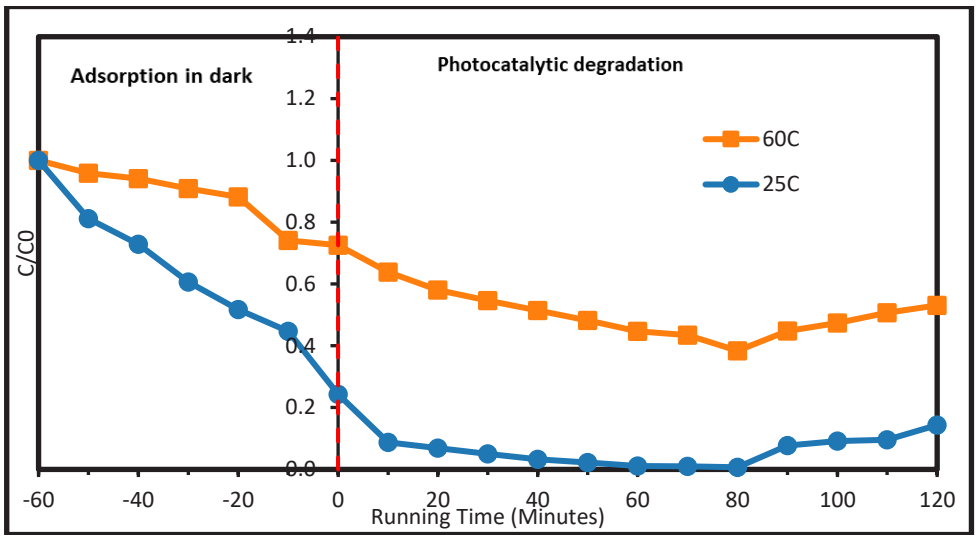


**Fig. 20**. Effect of reaction temperature on the photocatalytic degradation activity of MB dye for $Fe_3O_4/SiO_2/Ag_2VO_3$ at photocatalyst dose = 0.1 g/l, MB dye initial concentration = 40 ppm, initial pH = 10, and H2O2 concentration = 120 mM, reaction temperature=60 c,25c.

## 5.6. Effect of Light Intensity

The activation of the nanocomposite **$Fe_3O_4/SiO_2/AgVO_3$**, which is affected by the intensity of the light, leads to an increase in the creation of photoholes and electron re-excitation [2]. For methylene blue, the rate of oxidation is proportional to the light intensity [3]. The outcomes can be observed in Figure 21. In the study [13], researchers looked at three distinct light intensities: 50 W, 100 W, and 150 W. After comparing the degradation effectiveness at 50 W and 100 W, it was found that methylene blue was most successfully eliminated at 150 W. From 50 W to 100 W, the power saw a slowing of degradation and an increase in efficiency. Light intensity is directly proportional to photocatalytic efficiency, as the most effective elimination was attained at 150 W.

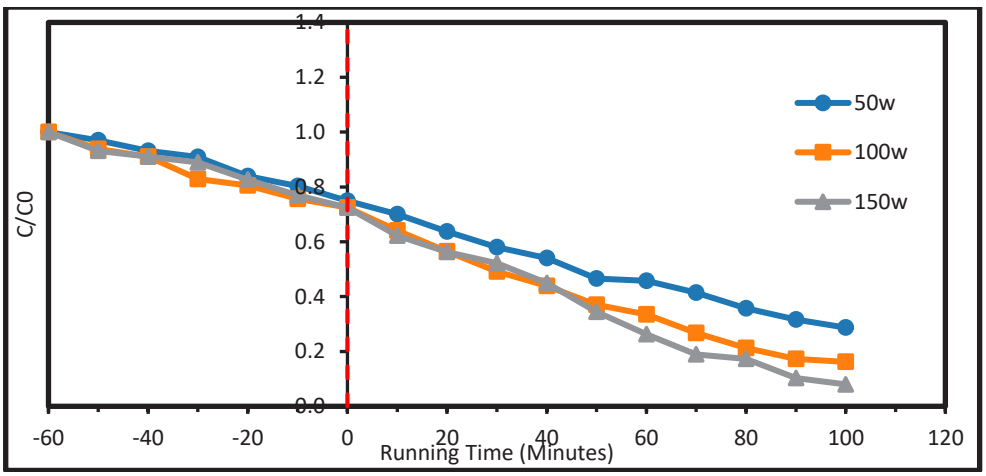


**Fig. 21.** Effect of Light Intensity on the photocatalytic degradation activity of MB dye for $Fe_3O_4/SiO_2/Ag_2VO_3$ at photocatalyst dose = 0.1 g/l, MB dye initial concentration = 40 ppm, initial pH = 10, and H2O2 concentration = 120 mM, Light Intensity =50 W, 100 W, and 150 W.

## 6. Reusability and Stability Studies

Research into stability and reusability is essential for demonstrating the long-term feasibility of photocatalytic applications and avoiding secondary contamination from recycled materials [12]. The outcomes of evaluating the stability and reusability of the $Fe_tO_4/SiO_2/Ag_2VO_3$ nanocomposite photocatalyst over five consecutive degradation cycles of Methylene Blue (MB) exposed to visible light are displayed in Figure 23(a and b). At the end of each cycle, the reaction mixture was magnetically stripped of the $Fe_3O_4/SiO_2/Ag_2VO_3$ photocatalyst, and the solvent was rinsed three times with ethanol to remove any remaining dye molecules and intermediate intermediates. Its reusability in the subsequent cycle was ensured by this action. Reusability measurements showed that the $Fe_tO_4/SiO_2/Ag_2VO_t$ nanocomposite maintained its photocatalytic activity even after many cycles. After a first-cycle MB removal efficiency of 99%, subsequent cycles saw drops to 98%, 93%, 91%, and 87%, respectively. After five cycles, the catalyst still maintained a considerable portion of its initial activity, proving its remarkable stability and resistance to photocorrosion. Reduced removal efficiency could be due to a number of factors, such as chemical intermediate surface fouling, partially blocked active sites, or insufficient catalyst loss during magnetic separation and washing. Figure 23(a) and (b) display the outcomes. The findings indicate that this $Fe_tO_4/SiO_2/Ag_2VO_t$ nanocomposite is stable and reusable, making it suitable for use in practical wastewater treatment. Prior research has shown that photocatalysts can remain stable and active for several cycles [13], [12].

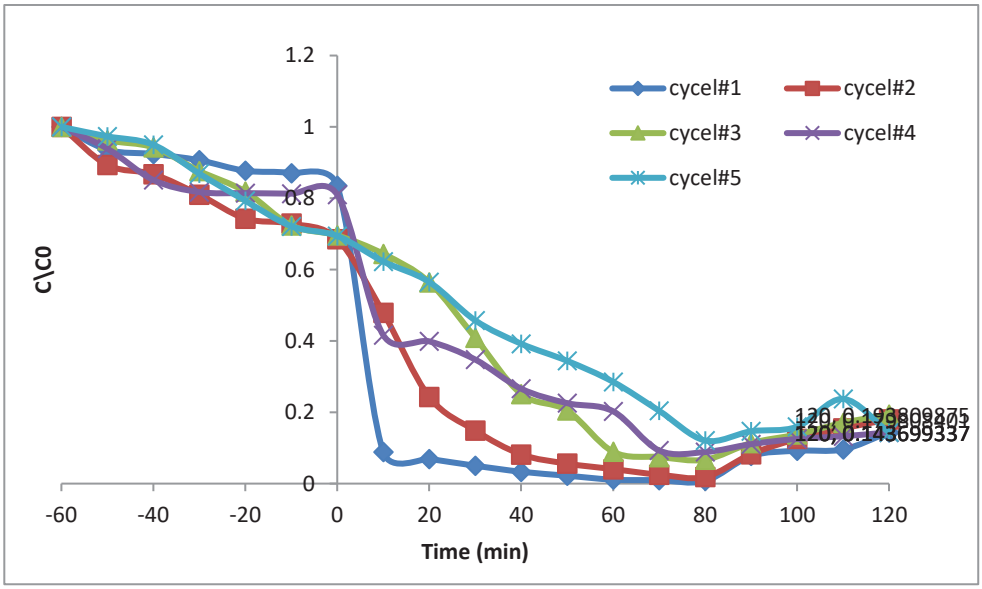


**Fig. 22** (a). Recyclability and stability studies of $Fe_3O_4/SiO_2/AgVO_3$ Supported Nanocomposite Photocatalysts under visible light irradiation system at photocatalyst dose = 0.1 g/l, MB dye initial concentration = 40 ppm, initial pH = 10, and H2O2 concentration =120mM.

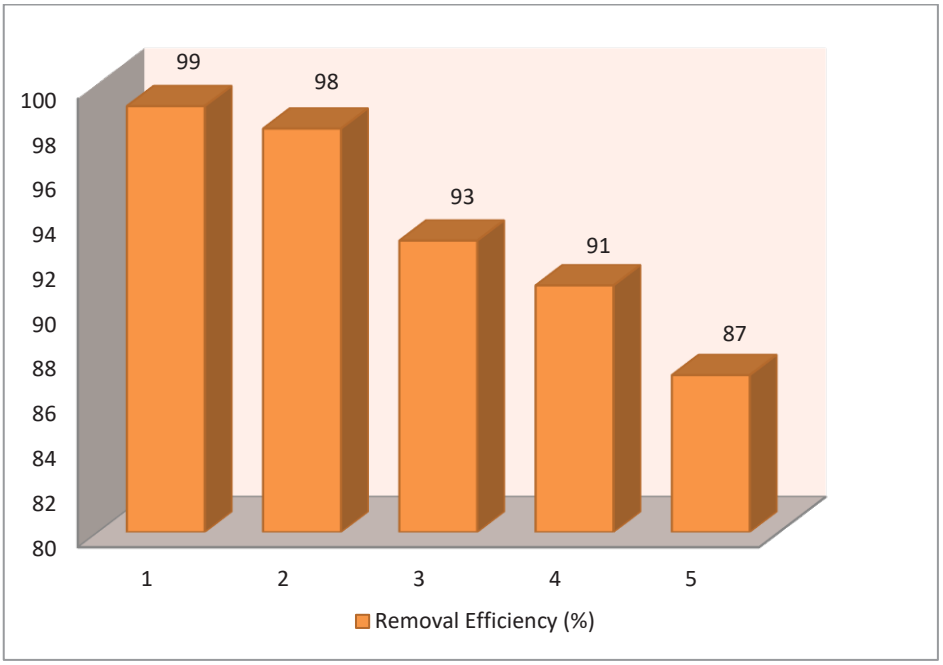


**Fig. 23(b).** Recyclability and stability studies of $Fe_3O_4/SiO_2/Ag_2VO_3$ Supported Nanocomposite Photocatalysts under visible light irradiation system at photocatalyst dose = 0.1 g/l, MB dye initial concentration = 40 ppm, initial pH = 10, and H2O2 concentration =120mM.

## 7. Scavenger Experiments

Investigating the roles of several active species (such as h+, e-, H2O2, • O2-, and • OH) in connection to the degradation of the MB dye might provide light on this photodegradation process. a component in the MB dye's breakdown. While this was going on, a nanocomposite of $Fe_tO_4/SiO_2/AgVO_t$ was used in many scavenging studies. Whereas, when "sodium oxalate, potassium dichromate, sodium-EDTA, P-benzoquinone, and isopropanol" were added at concentrations of 0.5 mmol/L, the photocatalytic degradation efficacy was 36%, 85%, 80%, 53%, and 72%, respectively. Researchers discovered that these chemicals could absorb h+, e, H2O2, • O2-, and • OH, three photoactive species. Figure 22 shows the outcomes of photocatalysis experiments using different scavengers. The primary objective of these research was to determine which photocatalytic species (such as h+ or OH) were critical for the decomposition of Rh B. Based on the results, it seems that hydroxyl (h+) and •OH radicals help oxidize MB; the potassium dichromate scavenger performed the best in this regard [13]. To determine the degree to which Methylene Blue (MB) mineralized during the photocatalytic process, we measured the chemical oxygen demand (COD). Continual oxygen demand (COD) is a crucial indication of water quality since it indicates the oxygen required to oxidize organic contaminants (Fertal, Young, & Oldacre, 2025). The change in COD and TOC readings before and after photocatalytic treatment utilizing the nanocomposite of $Fe_tO_4/SiO_2/Ag_2VO_t$ irradiated by visible light is shown in Figure 24. The Methylene Blue solution's COD value was around 400 mg/L at the beginning. Upon initial illumination, this level was 121 mg/L; however, it dropped to 131 mg/L following the first hour. A further reduction in COD level to 21.3 mg/L was achieved after 140 minutes of light therapy. Total organic carbon also decreased with time, from 40.3 mg/L after 0 minutes of illumination to 7.6 mg/L after 140 minutes of treatment. From the outset, we maintained a TOC level of 131 mg/L. The results show that the amount of organic contaminants in the solution was

significantly reduced by the photocatalytic process using the $Fe_tO_4/SiO_k/AgVO_3$ nanocomposite.

Total organic carbon (TOC) measures the concentration of carbon molecules in a sample, making it a good indicator of the presence of organic pollutants in water. Water and other organic compounds, such as aromatic molecules and amines, can have their carbon content determined using this method. A helpful indicator to check for when searching for organic contaminants that other metrics, like chemical oxygen demand (COD), could miss is total organic carbon (TOC). Researchers Shetty and Goyal (2022) measured total organic carbon (TOC) to find out how well the nanocomposite reduced organic pollutants using photocatalysis. Organic carbon concentrations in water, whether complex or simple, are typically determined using the total organic carbon (TOC) method (Fertal, Young, and Oldacre, 2025). This experiment tested the effectiveness of a photocatalytic treatment on a $Fe_3O_4/SiO_2/AgVO_3$ nanocomposite in decreasing organic pollutants by measuring total organic carbon (TOC). The first step was the transformation of total organic carbon (TOC) into total inorganic carbon (TIC). The following emissions of $CO_2$ and H2O will be released after the TIC conversion process. The oxidation process between the catalyst and the molecules was strengthened by the higher concentration of •OH in the MB effluent. It was observed that TIC oxidized to CO2 and H2O quite quickly. At the same time that TOC was transitioning, the processes that gave rise to TIC were also heavily involved in its development. The degradation rates of total organic carbon (TOC) and chemical oxygen demand (COD) must be considered when planning a photocatalytic treatment to remove the MB dye from wastewater. Depending on the duration of radiation exposure, the degradation rate of this reaction-stage varies.

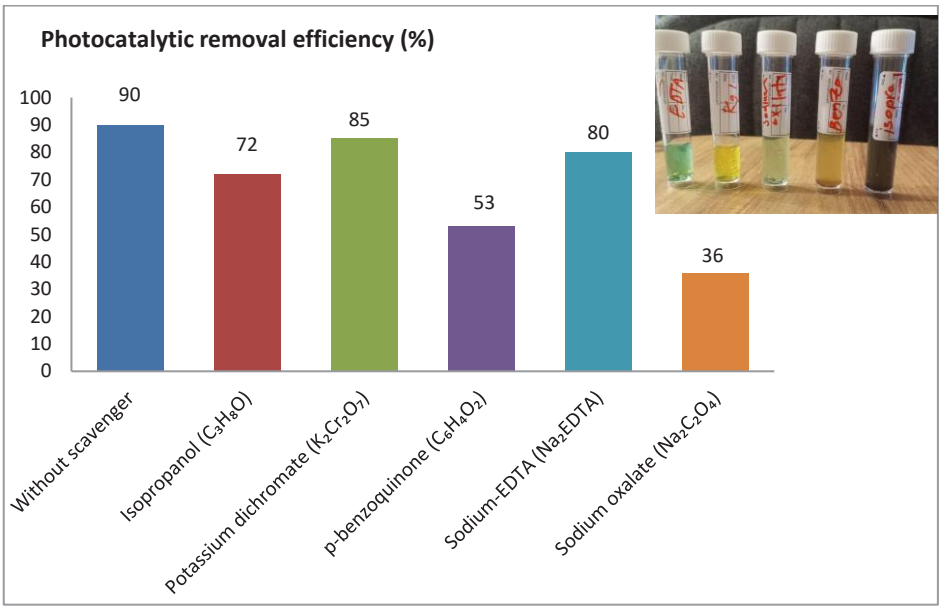


**Fig. 24.** Scavenger study by the addition of 0.5 mmol/L of each type.

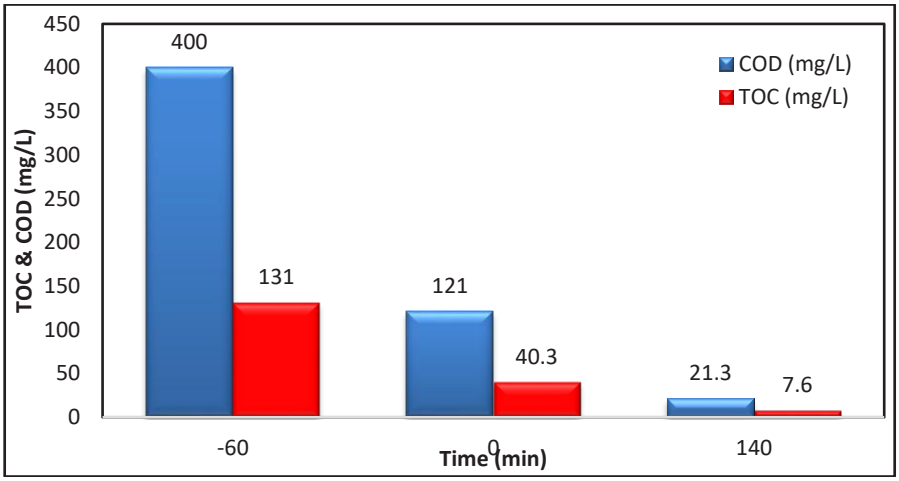


**Fig. 25.** Both TOC and COD values.

## 8. Conclusions

The purpose of this study was to create magnetic nanocomposites based on $Fe_3O_4$ and coated with $SiO_2$ and $AgVO_3$ using a green synthesis approach. The materials were intended to be magnetically recoverable and effective in removing pollutants from water. Synthesis of the supported nanocomposite took place. In order to reduce the employment of toxic chemicals, the synthesis method adhered to environmentally friendly principles in nanomaterial development and remediation. The improved accessibility of the active regions and the enhanced surface interaction with pollutant molecules are the reasons for the increased efficiency. As shown by magnetic measurements conducted using VSM, the nanocomposites that were formed retained strong magnetic properties. Quick magnetic separation and recovery from water-based solutions were both made possible by this. By demonstrating uniform particle distribution and the successful development of the coating layers, TEM morphological and structural examinations allowed us to establish the structural integrity of the supported and core-shell nanostructures. Incorporating the $SiO_2$ interlayer was critical for reducing particle agglomeration and increasing the dispersion of active components, which improved stability and functional performance. After confirming the nanocomposite's structural and physicochemical properties using several characterization processes, we looked at its potential practical applications using methylene blue dye as a model organic pollutant. Light intensity, starting pollutant concentration, nanocomposite dose, optimal hydrogen peroxide concentration, reaction temperature, and other critical operational parameters were all carefully examined to ascertain their effects. These studies found the optimal conditions for achieving the best possible removal performance. Extensive research on this $Fe_tO_4/SiO_k/AgVO_t$ nanocomposite has verified its efficacy and stability. By analyzing the surface area and interconnectivity, TEM and SEM confirm that the morphology is uniform with well-distributed $AgVO_3$ nanoparticles on silica-coated $Fe_3O_4$ cores. Stepwise functionalization is confirmed by FTIR spectra, which show Fe-O, Si-O-Si, and V-O bonds. Despite certain saturation magnetization losses due to surface coatings, VSM measurements reveal that the nanocomposite maintains its superparamagnetic properties. Without altering the core lattice, XRD analysis validates the coexistence of all phases by establishing the crystalline structure of $Fe_3O_4$ and integration of $AgVO_3$. Based on these findings, the nanocomposite may be a promising photocatalytic material due to its magnetic, structural, and morphological characteristics.

To further understand the reaction mechanism and identify the reactive species responsible for the degradation, scavenger tests were also carried out. Generally speaking, the eco-synthesized $Fe_tO_4/SiO_k$/AgVO3 nanocomposites demonstrated significant potential as sustainable and effective materials for state-of-the-art wastewater treatment. Because of its excellent reusability, structural stability, magnetic recoverability, and removal performance, the supported design stood out.

## References

1. N. Goodarzi, Z. Ashrafi-Peyman, E. Khani, A.Z. Moshfegh, Recent progress on semiconductor heterogeneous photocatalysts in clean energy production and environmental remediation. J. Clean. Prod. 13(7), 1102 (2023)
2. R.K. Paul, M. Ahmaruzzaman, Advanced photocatalytic degradation of POPs and other contaminants: A comprehensive review on nanocomposites and heterojunctions. RSC Adv. 15, 31313–31359 (2025). https://doi.org/10.1039/D5RA04336K
3. N. Harun, C.K. Sheng, M.G.M. Sabri et al., Impact of $TiO_2$ and $H_2O_2$ on photocatalytic degradation of Rhodamine B under ultraviolet C (UV-C) radiation for efficient polluted wastewater treatment. J. Optoelectron. Biomed. Mater. 12(1), 9–15 (2020)
4. I. Khan, K. Saeed, I. Zekker, B. Zhang, A.H. Hendi, A. Ahmad et al., Review on methylene blue: its properties, uses, toxicity, and photodegradation. Water 14(2), 242 (2022)
5. W. Mohammed, M. Matalkeh, R.M. Al Soubaihi, A. Elzatahry, K.M. Saoud, Visible light photocatalytic degradation of methylene blue dye and pharmaceutical wastes over ternary NiO/Ag/$TiO_2$ heterojunction. ACS Omega 8(43), 40063–40077 (2023)
6. M. Saraee, B. Maleki, T. Kikhavani, M. Mansouri, Investigating the process of photocatalytic removal of methylene blue from wastewater utilizing ZnO-Mn-Ce/Biochar nanocomposites under visible light. Int. J. Chem. Chem. Eng. Res. Adv. 43(12) (2024)
7. S.I.A. Shah, W. Ahmad, M. Anwar, R. Shah, J.A. Khan, N.S. Shah et al., Synthesis, properties, and applications of $Fe_3O_4$ and $Fe_3O_4$-based nanocomposites: A review. Adv. Colloid Interface Sci. 207049 (2025)
8. A. Shetty, A. Goyal, Total organic carbon analysis in water–A review of current methods. Mater. Today Proc. 65, 3881–3886 (2022)
9. J. Ramirez, Visible light-induced photocatalytic elimination of organic pollutants by $TiO_2$: A review. 65, 3881–3886 (2015)
10. N.A. Jasim, S.E. Ebrahim, S.H. Ammar, Fabrication of $Zn_xMn_{1-x}Fe_2O_4$ metal ferrites for boosted photocatalytic degradation of Rhodamine-B dye. Results Opt. 13, 100508 (2023)
11. N. Jasim, S. Ebrahim, S. Ammar, A comprehensive review on photocatalytic degradation of organic pollutants and microbial inactivation using Ag/$AgVO_3$ with metal ferrites based on magnetic nanocomposites. Cogent Eng. 10(1), 2228069 (2023). https://doi.org/10.1080/23311916.2023.2228069
12. N. Jasim, S. Ebrahim, S. Ammar, Photocatalytic degradation of Rhodamine B using $Co_xZn_{1-x}Fe_2O_4$ nanocomposite under visible light irradiation: Synthesis, characterization and its application. Alex. Eng. J. 82, 557–576 (2023). https://doi.org/10.1016/j.aej.2023.09.081
13. N. Jasim, S. Ammar, S. Ebrahim, Assembling $ZnMnFe_2O_4$@Ag-$AgVO_3$ nanostructure heterojunctions for photocatalytically degrading RhB and Pseudomonas aeruginosa bacteria under visible irradiation. J. Photochem. Photobiol. A: Chem. 449, 115380 (2023). https://doi.org/10.1016/j.jphotochem.2023.115380